Orbital-selective superconductivity in the pressurized bilayer nickelate La₃Ni₂O₇: An infinite projected entangled-pair state study

Jialin Chen [1,2] Fan Yang,[3,*] and Wei Li [1,2,†]

[1]*Institute of Theoretical Physics, Chinese Academy of Sciences, Beijing 100190, China*
[2]*Hefei National Laboratory, Hefei 230088, China*
[3]*School of Physics, Beijing Institute of Technology, Beijing 100081, China*

The newly discovered high-T_c nickelate superconductor La₃Ni₂O₇ has generated significant research interest. To uncover the pairing mechanism, it is essential to investigate the intriguing interplay between the two e_g, i.e., $d_{x^2-y^2}$ and d_{z^2} orbitals. Here we conduct an infinite projected entangled-pair state (iPEPS) study of the bilayer t-J model, directly in the thermodynamic limit and with orbitally selective parameters for $d_{x^2-y^2}$ and d_{z^2} orbitals, respectively. The $d_{x^2-y^2}$ electrons exhibit significant intralayer hopping $t_\parallel$ (and spin couplings $J_\parallel$) as well as strong interlayer $J_\perp$ passed from the d_{z^2} electrons. However, the interlayer $t_\perp$ is negligible in this case. In contrast, the d_{z^2} orbital demonstrates strong interlayer $t_\perp$ and $J_\perp$, while the inherent intralayer $t_\parallel$ and $J_\parallel$ are small. Based on the iPEPS results, we find clear orbital-selective behaviors in La₃Ni₂O₇. The $d_{x^2-y^2}$ orbitals exhibit robust superconductive (SC) order driven by the interlayer coupling $J_\perp$, while the d_{z^2} band shows relatively weak SC order as a result of small $t_\parallel$ (lack of coherence) but large $t_\perp$ (strong Pauli blocking). Furthermore, by substituting rare-earth element Pm or Sm with La, we find an enhanced SC order, which opens up a promising avenue for discovering nickelate superconductors with even higher T_c.

Introduction. The discovery of high-temperature superconductivity in the pressurized nickelate La₃Ni₂O₇ [1] has raised enthusiastic research interest both in experiment [2–7] and theory [8–49]. From a theoretical standpoint, the bilayer structure and orbital selectivity are two defining characteristics that set nickelate apart from cuprate superconductors. Despite significant advancements in the studies of pairing mechanisms using both weak- and strong-coupling approaches, there is still a debate regarding which of the two e_g orbitals [cf., Fig. 1(b)], $d_{x^2-y^2}$ [21,23–25] or d_{z^2} [26,30], is primarily responsible for the robust superconductivity in La₃Ni₂O₇.

Specifically, the d_{z^2} orbitals have strong interlayer hopping $t_\perp$ and negligible intralayer hopping $t_\parallel$ [8,9,13]. With strong renormalization due to Coulomb interactions [5,18], the d_{z^2} orbitals are local and have strong interlayer couplings. Thus a pair of electrons in the d_{z^2} orbitals can form a localized spin-singlet dimer. There are theoretical proposals that suggest a pathway towards SC order, which involve introducing holes into the rung singlets. Hybridization with neighboring e_g ($d_{x^2-y^2}$) orbitals provides the d_{z^2} holes with kinetic energy [14,26]. As a result, the tightly bound d_{z^2} hole pairs can move coherently within the bilayer system, giving rise to long-range SC order [30].

On the other hand, a contrasting viewpoint has been put forth that suggests the $d_{x^2-y^2}$ orbital is playing a major role in the formation of SC order in La₃Ni₂O₇ [21,23,25,32,36,37,39,43,47]. The Hund's rule coupling with a strength of about 1 eV in the system [15,18,31,45] plays a crucial role, which transfers the interlayer coupling $J_\perp$ from

the d_{z^2} orbital to the $d_{x^2-y^2}$ orbital through the symmetrization of spins on the two e_g orbitals located on the same site. Thus a bilayer $t_\parallel$-$J_\parallel$-$J_\perp$ model well describes the correlated $d_{x^2-y^2}$ electrons [21,23,25], which are found to host a robust and high-T_c SC order [21,25] driven by the strong antiferromagnetic (AFM) interlayer coupling $J_\perp$.

In this work, we employ the fermionic infinite projected entangled-pair state (iPEPS) approach, equipped with both simple updates (SU) and fast full updates (FFU), to study the bilayer t-J model, focusing on the SC orders in the two e_g orbitals. We compute the SC order parameters directly in the thermodynamic limit, going beyond the quasi-one-dimensional (quasi-1D) geometries in the previous density matrix renormalization group (DMRG) studies [14,25,46], where only quasi-long-range pairing correlations can be obtained. Based on the accurate 2D iPEPS calculations, we find that the $d_{x^2-y^2}$ band can be the dominant contributor to the s-wave SC order in La₃Ni₂O₇, while the d_{z^2} orbital has only very weak SC pairings. Additionally, we explore the possibility of substituting La with other rare-earth elements, and we find that the transition temperature T_c can be enhanced with Pm and Sm substitutions.

Bilayer t-J model for the $d_{x^2-y^2}$ and d_{z^2} orbitals. There are two e_g orbitals that we consider in the iPEPS calculations, the nearly half-filled d_{z^2} and quarter-filled $d_{x^2-y^2}$ orbitals, each described by a bilayer effective model [as depicted in Fig. 1(a)],

$$H_{\text{bilayer}} = -t_\parallel \sum_{\langle i,j\rangle,\mu,\sigma} (c^\dagger_{i,\mu,\sigma} c_{j,\mu,\sigma} + \text{H.c.})$$

$$+ J_\parallel \sum_{\langle i,j\rangle,\mu} \left(\mathbf{S}_{i,\mu} \cdot \mathbf{S}_{j,\mu} - \frac{1}{4} n_{i,\mu} n_{j,\mu} \right)$$

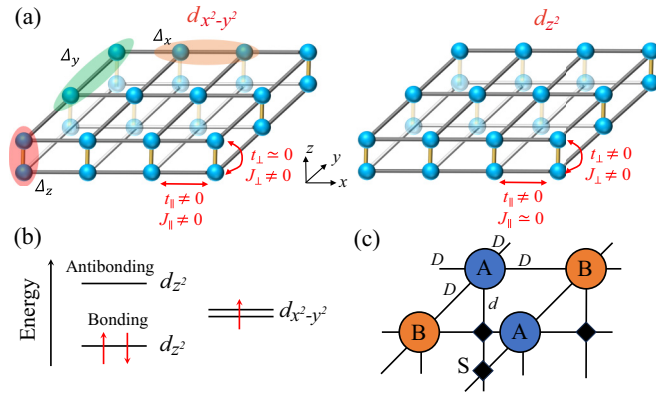*Contact author: yangfan_blg@bit.edu.cn
†Contact author: w.li@itp.ac.cn

FIG. 1. (a) The bilayer t-J model describing the behaviors of $d_{x^2-y^2}$ (left) and d_{z^2} (right) orbitals with properly chosen parameters. $d_{x^2-y^2}$ orbital has nonzero intralayer hopping $t_\parallel$, coupling $J_\parallel$, and effective interlayer coupling $J_\perp$, but without interlayer hopping $t_\perp$. d_{z^2} orbital has strong $t_\perp$, $J_\perp$ and effective $t_\parallel$. The SC pairing order parameters $\Delta_{x,y,z}$ are on the NN bonds along the x, y, and z axes, respectively (see definitions in the main text). Panel (b) illustrates the energy levels for the two e_g (d_{z^2} and $d_{x^2-y^2}$) orbitals of the two Ni$^{2.5+}$ ($3d^{7.5}$) cations in one unit cell of the bilayer La$_3$Ni$_2$O$_7$. Panel (c) illustrates the unit cell with two different bulk tensors (A and B) used in the fermionic iPEPS calculations shown in the main text. Swap gate S is introduced to account for fermion statistics, which equals -1 when two parity-odd indices cross, and 1 otherwise. D and d are the bond dimensions of the geometric and physical indices.

$$-t_\perp \sum_{i,\sigma} (c^\dagger_{i,\mu=1,\sigma} c_{i,\mu=-1,\sigma} + \text{H.c.})$$

$$+J_\perp \sum_i \mathbf{S}_{i,\mu=1} \cdot \mathbf{S}_{i,\mu=-1}, \tag{1}$$

where $c^\dagger_{i,\mu,\sigma}$ ($c_{i,\mu,\sigma}$) creates (annihilates) an electron of spin $\sigma = \{\uparrow, \downarrow\}$ at site i in layer $\mu = \{1, -1\}$, and the vector operator $\mathbf{S}_{i,\mu} = \frac{1}{2} c^\dagger_{i,\mu,\sigma} (\boldsymbol{\sigma}_{\sigma,\sigma'}) c_{i,\mu,\sigma'}$ denotes the spin of the electron with the Pauli matrices $\boldsymbol{\sigma} = \{\sigma_x, \sigma_y, \sigma_z\}$. $t_\parallel$ ($t_\perp$) is the intralayer (interlayer) hopping amplitude, and $J_\parallel$ ($J_\perp$) is the intralayer (interlayer) AFM coupling. The double occupancy is projected out in the bilayer t-J model as usual.

Based on the tight-binding model derived from density functional theory (DFT) calculations [8,28], we choose $t_\parallel = 1$ and $J_\parallel = 1/3$ for the $d_{x^2-y^2}$ orbital, together with interlayer $J_\perp = 2/3$ (while $t_\perp = 0$) passed from the d_{z^2} orbital [21,23,25]; on the other hand, for the d_{z^2} orbital we set $t_\perp = 1$ and $J_\perp = 2/3$ reflecting the strong σ bonding of d_{z^2} electrons, with effective $t_\parallel = 1/6$ (while $J_\parallel = 0$) gained from hybridization with $d_{x^2-y^2}$ orbitals [14,46]. We believe that the so-chosen parameters capture the essence of electron correlations in the two e_g orbitals of La$_3$Ni$_2$O$_7$.

Fermionic iPEPS method. To simulate the bilayer t-J model, we flatten the bilayer system into a single-layer system with enlarged local Hilbert space [25], and we employ the fermionic iPEPS method to simulate the ground state [50–59]. As illustrated in Fig. 1(c), we set a 2×2 unit cell with two bulk tensors A and B arranged periodically in the iPEPS wave function (larger unit cells produce consistent results; see the Supplemental Material [60]), and swap gates are introduced to encode the fermion statistics [53,54]. Each bulk tensor
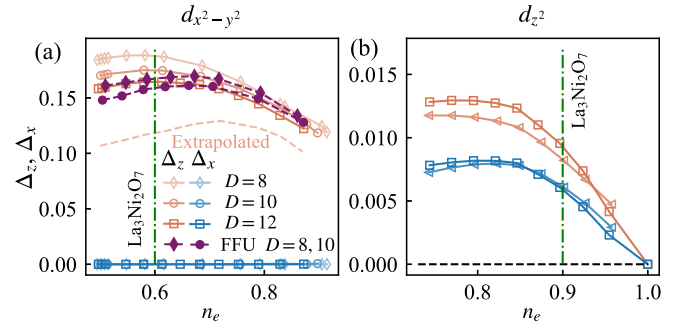

FIG. 2. The SC order parameters Δ_z for the interlayer pairing and Δ_x for the intralayer pairing, with varying electron density n_e for (a) $d_{x^2-y^2}$ and (b) d_{z^2} orbitals. Δ_y is found to be equal to Δ_x and thus not shown here. We retain D up to 12, and for $d_{x^2-y^2}$ we extrapolate Δ_z to the infinite-D limit [60]; for d_{z^2} orbital a good convergence is also reached, with SC order one order of magnitude smaller than that of the $d_{x^2-y^2}$ orbital. The green vertical lines mark different electron densities in the $d_{x^2-y^2}$ and d_{z^2} orbitals, where $n_{x^2-y^2} \simeq 0.6$ and $n_{z^2} \simeq 0.9$ in La$_3$Ni$_2$O$_7$. The model parameters are $t_\parallel = 1, J_\parallel = 1/3, t_\perp = 0$, $J_\perp = 2/3$ for $d_{x^2-y^2}$ orbital, and $t_\parallel = 1/6, J_\parallel = 0, t_\perp = 1, J_\perp = 2/3$ for d_{z^2} orbital.

has a physical bond with dimension $d = 9$ representing the direct product of two e_g orbitals with double occupancy projected out. The accuracy of our simulations is controlled by the geometric bond dimension D. We optimize the iPEPS wave function mainly using SU [54,61,62] with D retained up to 12 and further extrapolated to infinity. The FFU [63] is also exploited in the calculations, with bond dimension up to $D = 10$, and the results are in great agreement with SU results [60]. The expectation values are evaluated using the corner transfer matrix renormalization group method [64,65] with an environment bond dimension of $\chi = D^2$ that converges the results very well.

Orbital-selective superconductivity. In Fig. 2, we present the iPEPS results for the SC order parameters in the $d_{x^2-y^2}$ and d_{z^2} orbitals. The $d_{x^2-y^2}$ results are shown in Fig. 2(a), where we compute the interlayer SC order parameter $\Delta_z = \frac{1}{\sqrt{2}} \langle \sum_{\mu=\pm1} c^\dagger_{i,\mu,\uparrow} c^\dagger_{i,-\mu,\downarrow} \rangle$ with SU and find a strong interlayer pairing. By increasing the electron density n_e, Δ_z first increases and then decreases, with a large $\Delta_z = 0.13$ at the optimal density $n_e = 0.72$. To confirm the results, in Fig. 2 we also calculate Δ_z with FFU and find that the results agree with those of SU. These mutually corroborative results support a robust SC order in the $d_{x^2-y^2}$ orbital.

For electron density $n_{x^2-y^2} = 0.6$ relevant for the pristine compound La$_3$Ni$_2$O$_7$ [14,28,37,46,47], we find that the SC order parameter is $\Delta_z \simeq 0.12$, much greater than that in a plain 2D t-J model [64]. On the other hand, we find that the intralayer pairings, both Δ_x and Δ_y [see Fig. 1(a)], are negligible for all scanned electron densities. Here, $\Delta_{x(y)} = \frac{1}{\sqrt{2}} \sum_{\sigma=\{\uparrow,\downarrow\}} \langle \text{sgn}(\sigma) c^\dagger_{i,\mu,\sigma} c^\dagger_{i+\hat{x}(\hat{y}),\mu,\bar{\sigma}} \rangle$, with $\text{sgn}(\uparrow) = 1$, $\text{sgn}(\downarrow) = -1$, $\bar{\sigma}$ reverses the spin orientation of σ, and $\hat{x}(\hat{y})$ is the unit vector within the square-lattice plane (either $\mu = 1$ or -1).

The results for the d_{z^2} orbital are presented in Fig. 2(b). As the electron density decreases from 1.0 to about 0.75 (i.e., hole doped), the magnitudes of Δ_z and Δ_x (also Δ_y, not shown)
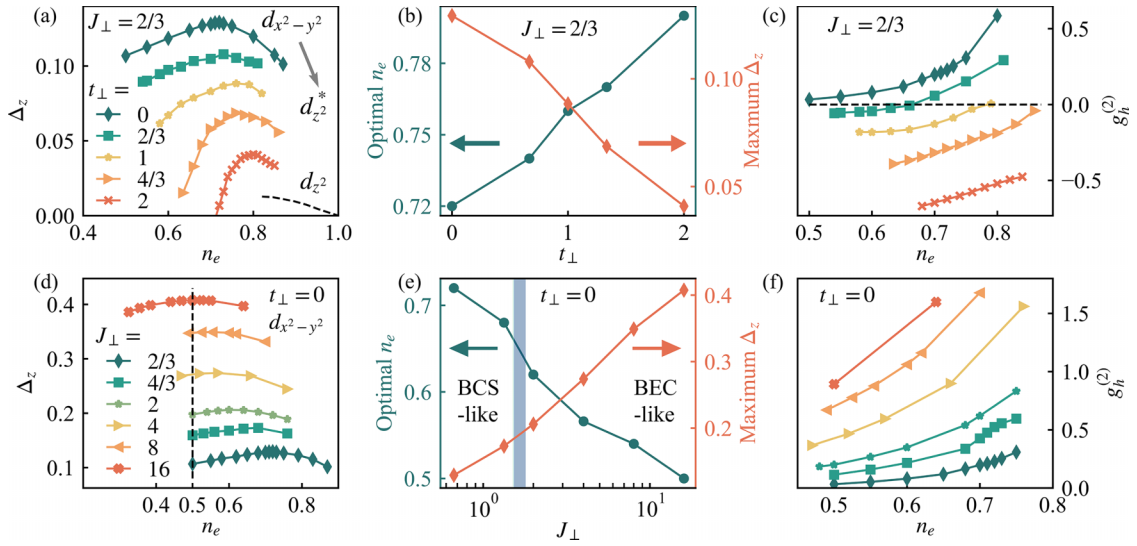
FIG. 3. The variation of interlayer SC order parameters Δ_z of $d_{x^2-y^2}$ orbital vs (a) $t_\perp$ and (d) $J_\perp$. The variations of maximal Δ_z and the corresponding optimal density n_e are plotted vs $t_\perp$ and $J_\perp$ in panels (b) and (e), respectively. By increasing $J_\perp$ for the $d_{x^2-y^2}$ orbital, a BCS-BEC crossover occurs in (e). Panels (c) and (f) show the evolution of interlayer hole correlations $g_h^{(2)}$ with n_e for different tuning parameters, with the same legends as those in (a) and (d), respectively. In panel (a), we increase $t_\perp$ and find it changes from $d_{x^2-y^2}$ orbital-like to a coherent d_{z^2} (denoted as $d_{z^2}^*$) behavior with weakened SC order. Besides $J_\perp$ and $t_\perp$, which are varying in the calculations, other model parameters are fixed as $t_\parallel = 1$, $J_\parallel = 1/3$, and all the results are extrapolated to infinity D [60]. As a comparison, we also plot the results for the d_{z^2} orbital taken from Fig. 1(b) with a dashed line, where the SC order is further reduced due to the smaller intralayer hopping $t_\parallel = 1/6$. The vertical dashed line in panel (d) indicates the quarter filling (i.e., $n = 0.5$), and the shaded bar in (e) represents the BCS-BEC crossover.

increase and then level off for $n_e \leqslant 0.85$ (cf., the $D = 10, 12$ data). The typical magnitude of Δ_z is about 0.01, one order smaller than that of the $d_{x^2-y^2}$ orbital shown in Fig. 2(a). These results indicate that the $d_{x^2-y^2}$ orbital contributes significantly more to the superconducting order in La$_3$Ni$_2$O$_7$, consistent with recent two-orbital model calculations [14,31,46,47].

Interlayer hopping and Pauli blocking. To understand the essential differences between the two e_g orbitals in La$_3$Ni$_2$O$_7$, we investigate the effects of the interlayer hopping $t_\perp$ and coupling $J_\perp$ on the SC order in Fig. 3.

To study the effect of $t_\perp$, we fix $t_\parallel = 1$, $J_\parallel = 1/3$, and $J_\perp = 2/3$, and we tune $t_\perp$ from 0 to 2. The results are presented in Figs. 3(a) and 3(b), where Δ_z reduces and the SC dome moves towards larger density n_e gradually with increasing $t_\perp$. We denote such a coherent d_{z^2} orbital as $d_{z^2}^*$, where we have artificially set a large $t_\parallel = 1$. One possible way to gain such kinetic energy is through the intersite hybridization with $d_{x^2-y^2}$ orbital. Nevertheless, even for $d_{z^2}^*$, the obtained values of Δ_z are still significantly weakened due to the large $t_\perp$, which lead to a reduction in the interlayer pairing, even under the presence of strong interlayer coupling $J_\perp$.

Moreover, we find that the SC order characterized by Δ_z is further reduced for the realistic d_{z^2} orbital with smaller, but also more realistic, intralayer hopping $t_\parallel = 1/6$. The above two factors well explain the orbital-selective superconductivity observed in recent numerical calculations of the two-orbital model [14,31,46].

To gain further insight into the effect of interlayer hopping $t_\perp$ on the SC pairing, we study the hole-hole correlation $g_h^{(2)} \equiv \langle h_{i,\mu=1} h_{i,\mu=-1} \rangle / (\langle h_{i,\mu=1} \rangle \langle h_{i,\mu=-1} \rangle) - 1$, where $h_{i,\mu} = 1 - n_{i,\mu}$ counts the hole number. The positive (negative) values of $g_h^{(2)}$ indicate bunching (antibunching) of the holes. In Fig. 3(c),

we observe that $g_h^{(2)}$ is always positive for $t_\perp = 0$, indicating the occurrence of hole bunching between two layers. However, as $t_\perp$ increases, $g_h^{(2)}$ decreases and may even cross the $g_h^{(2)} = 0$ line. This is because the interlayer hopping $t_\perp$ can introduce statistical repulsion between holes and is detrimental to interlayer pairing [66]. The electron density at the point where $g_h^{(2)}$ crosses zero gradually increases with increasing $t_\perp$ in Fig. 3(c), consistent with the observation that the SC dome moves towards larger n_e values as $t_\perp$ increases in Fig. 3(a).

Interlayer coupling driven BCS-BEC crossover. In the $d_{x^2-y^2}$ orbital scenario, the interlayer $J_\perp$ plays an essential role in driving the SC pairing. To reveal the advantage and explore the limit of the SC order in the $d_{x^2-y^2}$ orbital, in Figs. 3(d)–3(f) we present the results computed with model parameters $t_\parallel = 1$, $J_\parallel = 1/3$, and $t_\perp = 0$, similar to those used in Fig. 2(a), but with an increased AFM coupling $J_\perp$. In Fig. 3(d) we find that as $J_\perp$ increases, the interlayer SC order Δ_z increases and the SC dome shifts towards smaller n_e. To show the effect of $J_\perp$ more clearly, we collect the data and plot Δ_z versus $J_\perp$ in Fig. 3(e), and we observe that the maximum Δ_z increases drastically from about 0.13 to 0.41. The optimal n_e decreases from 0.72 to 0.5 (i.e., quarter-filling), in agreement with recent analytical results on the $t_\parallel$-$J_\parallel$-$J_\perp$ model [32,36].

The strong interlayer pairing in $d_{x^2-y^2}$ orbital can also be witnessed by the positive $g_h^{(2)}$ shown in Fig. 3(f), which represents a strong bunching between the two holes on the same interlayer vertical bond. We find that $g_h^{(2)}$ is always positive, and the hole bunching becomes greater as $J_\perp$ increases. For sufficiently large $J_\perp$, the hole pair changes from a loosely bounded Cooper pair, as in the Bardeen-Cooper-Schrieffer (BCS) theory, to a tightly bounded pair like a boson in the
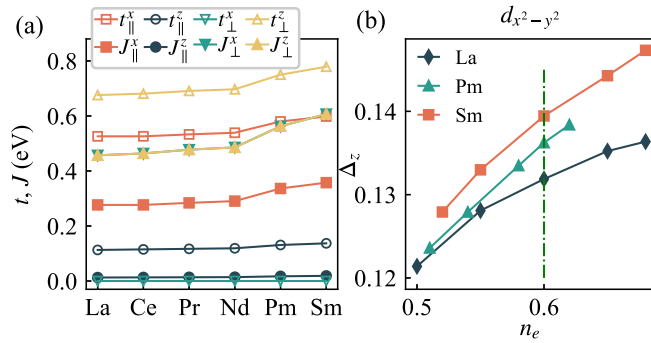
FIG. 4. (a) Hopping amplitudes and AFM couplings for the element substituted $R_3Ni_2O_7$ with R from La to Sm, and the superscript x (z) represents the $d_{x^2-y^2}$ (d_{z^2}) orbital. In the strong Hund's coupling limit, the interlayer AFM coupling can be fully passed from the d_{z^2} orbital to the $d_{x^2-y^2}$ one, namely, $J_\perp^x \equiv J_\parallel^z$ [21,25]. (b) The computed SC order parameter Δ_z vs density n_e for the $d_{x^2-y^2}$ orbital, with $R = $ La, Pm, and Sm. The green vertical line marks the estimated electron densities $n_e = 0.6$ for $R_3Ni_2O_7$. All SU results shown have been extrapolating to infinite D [60].

Bose-Einstein condensation (BEC). The maximal Δ_z appears at electron density $n = 0.5$, where the bosons gain the highest mobility. Therefore, the evolution of optimal density n_e from 0.72 to 0.5 indicates that a BCS-BEC crossover occurs by increasing $J_\perp$ [32], and the realistic value $J_\perp/t_\parallel \approx 2/3$ places the compound $La_3Ni_2O_7$ in the BCS side. These results highlight the potential of compounds with a similar bilayer structure to $La_3Ni_2O_7$ as a highly promising family of superconductors, with the possibility of achieving even higher T_c.

Mixed-dimensional bilayer pairing in $La_3Ni_2O_7$. In addition to the absence of coherent behavior and small hole densities that are essential in preventing the d_{z^2} orbital from achieving robust high-T_c superconductivity [21,47], we emphasize that the mixD bilayer structure is another critical factor that distinguishes the two e_g orbitals.

Specifically, for the d_{z^2} orbital the optimal electron density is close to half-filling, i.e., $\gtrsim 0.8$, similar to a conventional single-layer Hubbard or t-J system [64]. On the other hand, the $d_{x^2-y^2}$ orbital can be regarded to realize a mixD bilayer system [66,67], which has inter- and intralayer spin couplings $(J_\perp, J_\parallel)$ as well as intralayer hopping $t_\parallel$ but no interlayer hopping $t_\perp$. Such a mixD bilayer system benefits from a strong pairing force arising from the large AFM coupling $J_\perp$ and avoids the Pauli blocking due to the absence of interlayer $t_\perp$. As a result, the $d_{x^2-y^2}$ orbital with the mixD bilayer structure dominates in forming the SC order, which becomes progressively weakened as one approaches the more conventional bilayer structure of $d_{z^2}^*$ orbitals by increasing $t_\perp$ [see Fig. 3(a)].

Enhanced SC in $R_3Ni_2O_7$ *with element substitution.* Recently, DFT calculations showed that the *Fmmm* crystal structure is retained under pressure for rare-earth (RE) element substitution [28], where the hopping amplitudes and also exchange interactions can be enhanced [cf., Fig. 4(a)]. The authors in Ref. [28] further predicted that the pairing and T_c would decrease with such RE substitution from La to Sm, and that $La_3Ni_2O_7$ is already "optimal." On the other hand, in Ref. [37], a strong-coupling analysis based on slave

boson mean-field theory predicted that the RE substitution can significantly enhance the pairing strength and thus T_c, in sharp contrast to the weak-coupling analysis [28].

To settle this debate, we carry out iPEPS calculations with realistic parameters obtained from the DFT calculations [28] shown in Fig. 4(a). With properly chosen Coulomb interaction $U = 4$ eV [5,28,37], we estimate the AFM exchange interactions $J_\perp^z$ and $J_\parallel^z$ for the d_{z^2} orbital and $J_\parallel^x$ for the $d_{x^2-y^2}$ orbital according to the superexchange $J = 4t^2/U$. As shown in Fig. 4(b), the obtained SC order parameter Δ_z of the $d_{x^2-y^2}$ orbital increases when substituting La from Pm to Sm, at density $n_e = 0.6$ relevant for the nickelates. These results support that the SC pairing can be strengthened by element substitution, in agreement with the conclusion in Ref. [37] from the strong-coupling approach. By inspecting the hopping and coupling parameters in Fig. 4(a), we find that the enhancement of SC order mainly originates from the increased interlayer AFM interactions after the element substitution.

Discussion and outlook. In this work, we perform iPEPS simulations of the single-orbital bilayer t-J model for $d_{x^2-y^2}$ or d_{z^2} orbitals in $La_3Ni_2O_7$, directly in the thermodynamic limit, with corroborative simple and full update optimizations. Our results indicate that the interlayer superconducting order in the $d_{x^2-y^2}$ orbital is significantly stronger compared to that in the d_{z^2} orbital, due to the mixD bilayer structure that facilitates the SC order. The orbital selectivity originates from the different values of $t_\perp$ and $t_\parallel$ in the two orbitals, which have distinct effects on the SC order. $t_\perp$ can introduce Pauli blocking that is destructive for interlayer pairing, while a sufficiently large $t_\parallel$ is needed to render phase coherence for long-range SC order.

Our findings provide valuable insights for achieving higher critical temperatures T_c in superconductors with a mixD structure. Given the crucial role of inner-apical oxygen in modulating $J_\perp$ and the presence of oxygen vacancies in current $La_3Ni_2O_7$ samples [68], improving the sample quality and minimizing oxygen vacancies is a viable approach to enhancing the interlayer exchange $J_\perp$, and thereby increasing T_c. Moreover, our research encourages the exploration of more materials with a mixD structure, offering a promising avenue for discovering novel high-T_c superconductors.

We highlight the intriguing connections between two seemingly separate fields: the high-T_c nickelate superconductors and the optical lattice quantum simulations. In the latter, the mixD ladder system has been realized [66] and intensively discussed [39,41,43] recently. One possible extension of the present study is to include the $T > 0$ tensor-network calculations [69–75] relevant for the nickelate and quantum gas experiments.

Lastly, while our comparative study of the $d_{x^2-y^2}$ and d_{z^2} orbitals provides insights into the orbital-selective behaviors, a comprehensive two-orbital bilayer t-J model that includes both e_g orbitals is necessary to fully address their roles in $La_3Ni_2O_7$. There were attempts to study this interplay with DMRG calculations in ladder systems [14,46]. However, the study of two coupled infinite layers still poses significant challenges and is left for future studies.

[1] H. Sun, M. Huo, X. Hu, J. Li, Z. Liu, Y. Han, L. Tang, Z. Mao, P. Yang, B. Wang, J. Cheng, D.-X. Yao, G.-M. Zhang, and M. Wang, Signatures of superconductivity near 80 K in a nickelate under high pressure, Nature (London) **621**, 493 (2023).

[2] Z. Liu, M. Huo, J. Li, Q. Li, Y. Liu, Y. Dai, X. Zhou, J. Hao, Y. Lu, M. Wang, and H.-H. Wen, Electronic correlations and partial gap in the bilayer nickelate $La_3Ni_2O_7$, arXiv:2307.02950.

[3] J. Hou, P.-T. Yang, Z.-Y. Liu, J.-Y. Li, P.-F. Shan, L. Ma, G. Wang, N.-N. Wang, H.-Z. Guo, J.-P. Sun, Y. Uwatoko, M. Wang, G.-M. Zhang, B.-S. Wang, and J.-G. Cheng, Emergence of high-temperature superconducting phase in pressurized $La_3Ni_2O_7$ crystals, Chin. Phys. Lett. **40**, 117302 (2023).

[4] Y. Zhang, D. Su, Y. Huang, Z. Shan, H. Sun, M. Huo, K. Ye, J. Zhang, Z. Yang, Y. Xu, Y. Su, R. Li, M. Smidman, M. Wang, L. Jiao, and H. Yuan, High-temperature superconductivity with zero resistance and strange-metal behaviour in $La_3Ni_2O_{7-\delta}$, Nat. Phys. (2024).

[5] J. Yang, H. Sun, X. Hu, Y. Xie, T. Miao, H. Luo, H. Chen, B. Liang, W. Zhu, G. Qu, C.-Q. Chen, M. Huo, Y. Huang, S. Zhang, F. Zhang, F. Yang, Z. Wang, Q. Peng, H. Mao, G. Liu *et al.*, Orbital-dependent electron correlation in double-layer nickelate $La_3Ni_2O_7$, Nat. Commun. **15**, 4373 (2024).

[6] M. Zhang, C. Pei, Q. Wang, Y. Zhao, C. Li, W. Cao, S. Zhu, J. Wu, and Y. Qi, Effects of pressure and doping on Ruddlesden-Popper phases $La_{n+1}Ni_nO_{3n+1}$, J. Mater. Sci. Technol. **185**, 147 (2024).

[7] G. Wang, N. N. Wang, X. L. Shen, J. Hou, L. Ma, L. F. Shi, Z. A. Ren, Y. D. Gu, H. M. Ma, P. T. Yang, Z. Y. Liu, H. Z. Guo, J. P. Sun, G. M. Zhang, S. Calder, J.-Q. Yan, B. S. Wang, Y. Uwatoko, and J.-G. Cheng, Pressure-induced superconductivity in polycrystalline $La_3Ni_2O_{7-\delta}$, Phys. Rev. X **14**, 011040 (2024).

[8] Z. Luo, X. Hu, M. Wang, W. Wú, and D.-X. Yao, Bilayer two-orbital model of $La_3Ni_2O_7$ under pressure, Phys. Rev. Lett. **131**, 126001 (2023).

[9] Y. Zhang, L.-F. Lin, A. Moreo, and E. Dagotto, Electronic structure, dimer physics, orbital-selective behavior, and magnetic tendencies in the bilayer nickelate superconductor $La_3Ni_2O_7$ under pressure, Phys. Rev. B **108**, L180510 (2023).

[10] Q.-G. Yang, D. Wang, and Q.-H. Wang, Possible $s_\pm$-wave superconductivity in $La_3Ni_2O_7$, Phys. Rev. B **108**, L140505 (2023).

[11] F. Lechermann, J. Gondolf, S. Bötzel, and I. M. Eremin, Electronic correlations and superconducting instability in $La_3Ni_2O_7$ under high pressure, Phys. Rev. B **108**, L201121 (2023).

[12] H. Sakakibara, N. Kitamine, M. Ochi, and K. Kuroki, Possible High T_c superconductivity in $La_3Ni_2O_7$ under high pressure through manifestation of a nearly half-filled bilayer Hubbard model, Phys. Rev. Lett. **132**, 106002 (2024).

[13] Y. Gu, C. Le, Z. Yang, X. Wu, and J. Hu, Effective model and pairing tendency in bilayer Ni-based superconductor $La_3Ni_2O_7$, arXiv:2306.07275.

[14] Y. Shen, M. Qin, and G.-M. Zhang, Effective Bi-layer model Hamiltonian and density-matrix renormalization group study for the high-T_c superconductivity in $La_3Ni_2O_7$ under high pressure, Chin. Phys. Lett. **40**, 127401 (2023).

[15] V. Christiansson, F. Petocchi, and P. Werner, Correlated electronic structure of $La_3Ni_2O_7$ under pressure, Phys. Rev. Lett. **131**, 206501 (2023).

[16] D. A. Shilenko and I. V. Leonov, Correlated electronic structure, orbital-selective behavior, and magnetic correlations in double-layer $La_3Ni_2O_7$ under pressure, Phys. Rev. B **108**, 125105 (2023).

[17] W. Wú, Z. Luo, D.-X. Yao, and M. Wang, Superexchange and charge transfer in the nickelate superconductor $La_3Ni_2O_7$ under pressure, Sci. China Phys. Mech. Astron. **67**, 117402 (2024).

[18] Y. Cao and Y.-F. Yang, Flat bands promoted by Hund's rule coupling in the candidate double-layer high-temperature superconductor $La_3Ni_2O_7$ under high pressure, Phys. Rev. B **109**, L081105 (2024).

[19] X. Chen, P. Jiang, J. Li, Z. Zhong, and Y. Lu, Critical charge and spin instabilities in superconducting $La_3Ni_2O_7$, arXiv:2307.07154.

[20] Y.-B. Liu, J.-W. Mei, F. Ye, W.-Q. Chen, and F. Yang, $s^\pm$-wave pairing and the destructive role of apical-oxygen deficiencies in $La_3Ni_2O_7$ under pressure, Phys. Rev. Lett. **131**, 236002 (2023).

[21] C. Lu, Z. Pan, F. Yang, and C. Wu, Interlayer-coupling-driven high-temperature superconductivity in $La_3Ni_2O_7$ under pressure, Phys. Rev. Lett. **132**, 146002 (2024).

[22] Y. Zhang, L.-F. Lin, A. Moreo, T. A. Maier, and E. Dagotto, Structural phase transition, $s_\pm$-wave pairing, and magnetic stripe order in bilayered superconductor $La_3Ni_2O_7$ under pressure, Nat. Commun. **15**, 2470 (2024).

[23] H. Oh and Y.-H. Zhang, Type-II $t - J$ model and shared superexchange coupling from Hund's rule in superconducting $La_3Ni_2O_7$, Phys. Rev. B **108**, 174511 (2023).

[24] Z. Liao, L. Chen, G. Duan, Y. Wang, C. Liu, R. Yu, and Q. Si, Electron correlations and superconductivity in $La_3Ni_2O_7$ under pressure tuning, Phys. Rev. B **108**, 214522 (2023).

[25] X.-Z. Qu, D.-W. Qu, J. Chen, C. Wu, F. Yang, W. Li, and G. Su, Bilayer $t - J - J_\perp$ model and magnetically mediated pairing in the pressurized nickelate $La_3Ni_2O_7$, Phys. Rev. Lett. **132**, 036502 (2024).

[26] Y.-F. Yang, G.-M. Zhang, and F.-C. Zhang, Interlayer valence bonds and two-component theory for high-T_c superconductivity of $La_3Ni_2O_7$ under pressure, Phys. Rev. B **108**, L201108 (2023).

[27] K. Jiang, Z. Wang, and F.-C. Zhang, High-temperature superconductivity in $La_3Ni_2O_7$, Chin. Phys. Lett. **41**, 017402 (2024).

[28] Y. Zhang, L.-F. Lin, A. Moreo, T. A. Maier, and E. Dagotto, Trends in electronic structures and $s_\pm$-wave pairing for the rare-earth series in bilayer nickelate superconductor $R_3Ni_2O_7$, Phys. Rev. B **108**, 165141 (2023).

[29] J. Huang, Z. D. Wang, and T. Zhou, Impurity and vortex states in the bilayer high-temperature superconductor $La_3Ni_2O_7$, Phys. Rev. B **108**, 174501 (2023).

[30] Q. Qin and Y.-F. Yang, High-T_c superconductivity by mobilizing local spin singlets and possible route to higher T_c in pressurized $La_3Ni_2O_7$, Phys. Rev. B **108**, L140504 (2023).

[31] Y.-H. Tian, Y. Chen, J.-M. Wang, R.-Q. He, and Z.-Y. Lu, Correlation effects and concomitant two-orbital $s_\pm$-wave superconductivity in $La_3Ni_2O_7$ under high pressure, Phys. Rev. B **109**, 165154 (2024).

[32] D.-C. Lu, M. Li, Z.-Y. Zeng, W. Hou, J. Wang, F. Yang, and Y.-Z. You, Superconductivity from doping symmetric mass generation insulators: Application to $La_3Ni_2O_7$ under pressure, arXiv:2308.11195.

[33] R. Jiang, J. Hou, Z. Fan, Z.-J. Lang, and W. Ku, Pressure driven fractionalization of ionic spins results in cupratelike high-T_c superconductivity in $La_3Ni_2O_7$, Phys. Rev. Lett. **132**, 126503 (2024).

[34] N. Kitamine, M. Ochi, and K. Kuroki, Theoretical designing of multiband nickelate and palladate superconductors with $d^{8+\delta}$ configuration, arXiv:2308.12750.

[35] Z. Luo, B. Lv, M. Wang, W. Wú, and D.-X. Yao, High-T_C superconductivity in $La_3Ni_2O_7$ based on the bilayer two-orbital t-J model, arXiv:2308.16564.

[36] J.-X. Zhang, H.-K. Zhang, Y.-Z. You, and Z.-Y. Weng, Strong pairing originated from an emergent $\mathbb{Z}_2$ Berry phase in $La_3Ni_2O_7$, arXiv:2309.05726.

[37] Z. Pan, C. Lu, F. Yang, and C. Wu, Effect of rare-earth element substitution in superconducting $R_3Ni_2O_7$ under pressure, arXiv:2309.06173.

[38] H. Sakakibara, M. Ochi, H. Nagata, Y. Ueki, H. Sakurai, R. Matsumoto, K. Terashima, K. Hirose, H. Ohta, M. Kato, Y. Takano, and K. Kuroki, Theoretical analysis on the possibility of superconductivity in the trilayer Ruddlesden-Popper nickelate $La_4Ni_3O_{10}$ under pressure and its experimental examination: Comparison with $La_3Ni_2O_7$, Phys. Rev. B **109**, 144511 (2024).

[39] H. Lange, L. Homeier, E. Demler, U. Schollwöck, A. Bohrdt, and F. Grusdt, Pairing dome from an emergent Feshbach resonance in a strongly repulsive bilayer model, arXiv:2309.13040.

[40] B. Geisler, J. J. Hamlin, G. R. Stewart, R. G. Hennig, and P. J. Hirschfeld, Structural transitions, octahedral rotations, and electronic properties of $A_3Ni_2O_7$ rare-earth nickelates under high pressure, npj Quantum Mater. **9**, 38 (2024).

[41] H. Yang, H. Oh, and Y.-H. Zhang, Strong pairing from small Fermi surface beyond weak coupling: Application to $La_3Ni_2O_7$, arXiv:2309.15095.

[42] L. C. Rhodes and P. Wahl, Structural routes to stabilize superconducting $La_3Ni_2O_7$ at ambient pressure, Phys. Rev. Mater. **8**, 044801 (2024).

[43] H. Lange, L. Homeier, E. Demler, U. Schollwöck, F. Grusdt, and A. Bohrdt, Feshbach resonance in a strongly repulsive bilayer model: A possible scenario for bilayer nickelate superconductors, arXiv:2309.15843.

[44] H. LaBollita, V. Pardo, M. R. Norman, and A. S. Botana, Electronic structure and magnetic properties of $La_3Ni_2O_7$ under pressure: active role of the Ni-$d_{x^2-y^2}$ orbitals, arXiv:2309.17279.

[45] U. Kumar, C. Melnick, and G. Kotliar, Softening of dd excitation in the resonant inelastic x-ray scattering spectra as a signature of Hund's coupling in nickelates, arXiv:2310.00983.

[46] T. Kaneko, H. Sakakibara, M. Ochi, and K. Kuroki, Pair correlations in the two-orbital Hubbard ladder: Implications for superconductivity in the bilayer nickelate $La_3Ni_2O_7$, Phys. Rev. B **109**, 045154 (2024).

[47] C. Lu, Z. Pan, F. Yang, and C. Wu, Interplay of two E_g orbitals in superconducting $La_3Ni_2O_7$ under pressure, arXiv:2310.02915.

[48] S. Ryee, N. Witt, and T. O. Wehling, Quenched pair breaking by interlayer correlations as a key to superconductivity in $La_3Ni_2O_7$, arXiv:2310.17465v3.

[49] H. Schlömer, U. Schollwöck, F. Grusdt, and A. Bohrdt, Superconductivity in the pressurized nickelate $La_3Ni_2O_7$ in the vicinity of a BEC-BCS crossover, arXiv:2311.03349.

[50] F. Verstraete and J. I. Cirac, Renormalization algorithms for quantum-many body systems in two and higher dimensions, arXiv:cond-mat/0407066.

[51] J. Jordan, R. Orús, G. Vidal, F. Verstraete, and J. I. Cirac, Classical simulation of infinite-size quantum lattice systems in two spatial dimensions, Phys. Rev. Lett. **101**, 250602 (2008).

[52] J. I. Cirac, D. Pérez-García, N. Schuch, and F. Verstraete, Matrix product states and projected entangled pair states: Concepts, symmetries, theorems, Rev. Mod. Phys. **93**, 045003 (2021).

[53] P. Corboz and G. Vidal, Fermionic multiscale entanglement renormalization ansatz, Phys. Rev. B **80**, 165129 (2009).

[54] P. Corboz, R. Orús, B. Bauer, and G. Vidal, Simulation of strongly correlated fermions in two spatial dimensions with fermionic projected entangled-pair states, Phys. Rev. B **81**, 165104 (2010).

[55] T. Barthel, C. Pineda, and J. Eisert, Contraction of fermionic operator circuits and the simulation of strongly correlated fermions, Phys. Rev. A **80**, 042333 (2009).

[56] C. V. Kraus, N. Schuch, F. Verstraete, and J. I. Cirac, Fermionic projected entangled pair states, Phys. Rev. A **81**, 052338 (2010).

[57] P. Corboz, P. Czarnik, G. Kapteijns, and L. Tagliacozzo, Finite correlation length scaling with infinite projected entangled-pair states, Phys. Rev. X **8**, 031031 (2018).

[58] M. M. Rams, P. Czarnik, and L. Cincio, Precise extrapolation of the correlation function asymptotics in uniform tensor network states with application to the Bose-Hubbard and XXZ models, Phys. Rev. X **8**, 041033 (2018).

[59] M. Rader and A. M. Läuchli, Finite correlation length scaling in Lorentz-invariant gapless iPEPS wave functions, Phys. Rev. X **8**, 031030 (2018).

[60] See Supplemental Material at http://link.aps.org/supplemental/10.1103/PhysRevB.110.L041111 for additional details. In Supplemental Sec. I, we provide the details and comparisons between the SU and FFU. In Secs. II and III, we show the process for extrapolating the SC order parameters obtained from a simple update to the infinite-D limit, for pristine and rare-earth element substituted nickelate $R_3Ni_2O_7$. In Sec. IV, we provide results for larger iPEPS unit cells and comparisons among them.

[61] H. C. Jiang, Z. Y. Weng, and T. Xiang, Accurate determination of tensor network state of quantum lattice models in two dimensions, Phys. Rev. Lett. **101**, 090603 (2008).

[62] W. Li, J. von Delft, and T. Xiang, Efficient simulation of infinite tree tensor network states on the Bethe lattice, Phys. Rev. B **86**, 195137 (2012).

[63] H. N. Phien, J. A. Bengua, H. D. Tuan, P. Corboz, and R. Orús, Infinite projected entangled pair states algorithm improved: Fast full update and gauge fixing, Phys. Rev. B **92**, 035142 (2015).

[64] P. Corboz, T. M. Rice, and M. Troyer, Competing states in the t-J model: Uniform d-wave state versus stripe state, Phys. Rev. Lett. **113**, 046402 (2014).

[65] R. Orús and G. Vidal, Simulation of two-dimensional quantum systems on an infinite lattice revisited: Corner transfer matrix for tensor contraction, Phys. Rev. B **80**, 094403 (2009).

[66] S. Hirthe, T. Chalopin, D. Bourgund, P. Bojović, A. Bohrdt, E. Demler, F. Grusdt, I. Bloch, and T. A. Hilker, Magnetically mediated hole pairing in fermionic ladders of ultracold atoms, Nature (London) **613**, 463 (2023).

[67] A. Bohrdt, L. Homeier, I. Bloch, E. Demler, and F. Grusdt, Strong pairing in mixed-dimensional bilayer antiferromagnetic Mott insulators, Nat. Phys. **18**, 651 (2022).

[68] Z. Dong, M. Huo, J. Li, J. Li, P. Li, H. Sun, L. Gu, Y. Lu, M. Wang, Y. Wang, and Z. Chen, Visualization of oxygen vacancies and self-doped ligand holes in $La_3Ni_2O_{7-\delta}$, Nature (London) **630**, 847 (2024).

[69] W. Li, S.-J. Ran, S.-S. Gong, Y. Zhao, B. Xi, F. Ye, and G. Su, Linearized tensor renormalization group algorithm for the calculation of thermodynamic properties of quantum lattice models, Phys. Rev. Lett. **106**, 127202 (2011).

[70] Y.-L. Dong, L. Chen, Y.-J. Liu, and W. Li, Bilayer linearized tensor renormalization group approach for thermal tensor networks, Phys. Rev. B **95**, 144428 (2017).

[71] Q. Li, Y. Gao, Y.-Y. He, Y. Qi, B.-B. Chen, and W. Li, Tangent space approach for thermal tensor network simulations of the 2D Hubbard model, Phys. Rev. Lett. **130**, 226502 (2023).

[72] S. R. White, Minimally entangled typical quantum states at finite temperature, Phys. Rev. Lett. **102**, 190601 (2009).

[73] E. M. Stoudenmire and S. R. White, Minimally entangled typical thermal state algorithms, New J. Phys. **12**, 055026 (2010).

[74] P. Czarnik and J. Dziarmaga, Fermionic projected entangled pair states at finite temperature, Phys. Rev. B **90**, 035144 (2014).

[75] P. Czarnik, M. M. Rams, and J. Dziarmaga, Variational tensor network renormalization in imaginary time: Benchmark results in the Hubbard model at finite temperature, Phys. Rev. B **94**, 235142 (2016).